

Design of a novel three phase hybrid converter for microgrids application using renewable energy sources

Bhukya Devulal^{1,2}, Manickam Siva¹, Dasari Ravi Kumar²

¹Department of Electrical and Electronics Engineering, Annamalai University, Chidambaram, India

²Department of Electrical and Electronics Engineering, VNR Vignana Jyothi Institute of Engineering and Technology Hyderabad, Telangana, India

Article Info

Article history:

Received Jul 22, 2024

Revised Nov 5, 2024

Accepted Nov 20, 2024

Keywords:

Hybrid H-bridge inverter

Multi-level inverter

Pulse width-modulation

Renewable energy sources

Total harmonic distortion

ABSTRACT

A multi-level inverter (MLI) plays a vital role in recent days with an increasing trend of usage of microgrid and distributed generator. MLIs are popular in high voltage and high-power applications. MLIs operate with dominant switching frequency pulse width-modulation (PWM) techniques. These MLIs not only generate the output voltage with fewer harmonics but also reduce the dV/dt stress on switches. The induction machine connected to these MLIs, adds greater advantages in real time applications. This paper presents a novel 13 and 21-level hybrid H-bridge inverter (HHBI) connected to induction drive by using a photovoltaic module for microgrid applications using maximum power point tracking (MPPT) through a PV array. Hybrid H-bridge inverters combine elements from different inverter topologies to optimize appearance in terms of efficiency, harmonics and system complexity. The main aim is to reduce harmonics using high level of inverter and by controlling motor characteristics. Here a novel PWM control method is used for making the exchanging sequences for the corresponding switches. From the MATLAB results presented, it can be noticed that with the proposed methodology the THD is reduced to 4.66 and number of switches to 39, which reduces the complexity of the system. It also minimized the switching losses and increases efficiency.

This is an open access article under the [CC BY-SA](https://creativecommons.org/licenses/by-sa/4.0/) license.



Corresponding Author:

Bhukya Devulal

Department of Electrical and Electronics Engineering, Annamalai University

Chidambaram, Tamil Nadu, India

E-mail: devulalb@gmail.com

1. INTRODUCTION

Multi-level inverters are playing a vital role in recent day's applications with an increasing usage of renewable energy sources [1]–[3]. These inverters are also helpful in micro grid applications. There are two levels of inverter with voltages +V and -V, these two levels of voltage changed from pulse width-modulation (PWM) technique strategy make successful harmonics distortion, EMI and dV/dt stress [4], [5].

Various multilevel inverter topologies given in [6]–[9]. Major multi-level inverter (MLI) topologies with cascaded H-bridges are considered in studies [10], [11]. Each of these configurations utilizes distinct approaches for voltage modulation, employing either separate DC sources, diode clamps, or flying capacitors for achieving multilevel output waveforms. Multi-level inverter incorporates several ideal power switches with a combination of capacitor and flying diode, expanding the quantity of voltage levels [12]. Cascaded hybrid multi-inverters are planned with a different direct current (DC) voltage source and are productive to utilize when contrasted. Since there is no need of capacitors and diodes here and it additionally utilizes distinctive unbalanced voltage sources from renewable energy sources like fuel cell, sunlight-based cell and

wind energy [13]. More voltage levels are possible to be accomplished by inserting more H-bridges which produces smooth sinusoidal waveform with a lower total harmonic distortion (THD) proportion [14], [15].

The novel inverter topology provides a significant advancement in multilevel inverter technology for solar PV systems [9]. It offers a promising solution for improving the cost-effectiveness and performance of renewable energy systems. The inverter can function as a three-stage direct current (DC) to alternating current (AC) inverter, AC to AC inverter, and it can use system and PV power directly [16], [17]. Explores symmetrical concealment, PWM systems, and their benefits and drawbacks. It also discusses various PWM methods, their advantages and disadvantages, and future projections. The development of hybrid micro-grids for residential use that integrate the AC energy grid, electric car charging stations, and renewable energy sources. New solar inverters enable local energy storage for renewable energy sources with this model [18].

Renewable energy-based microgrids, such as AC and DC, are effective in addressing energy crises and environmental issues. DC-dominated hybrid microgrids combine advantages of both types, but require proper power coordination control for stable operation [19]–[22]. Discusses commonly applied control techniques for hybrid microgrids. A model predictive control (MPC)-based distributed control algorithm is given in [23] for hybrid AC/DC microgrids. It analyzes grid conditions and designates BIC to regulate the highest deviated parameter in nonlinear conditions. The study in [24] presents a transformer-less DC-DC power boost converter with a switched-capacitor structure and sliding mode controller (SMC) for PV applications. The converter increases DC voltage gain and reduces voltage stress on the power switch, allowing longer off-time for continuous current mode operations. The converter's control process is simpler compared to multi-switched topologies.

The Arvin converter given in [25] offers numerous advantages, including a common ground-based high-gain topology, a simple fuzzy logic controller, bidirectional energy flow, cost-effectiveness, and a reduced number of semiconductor devices and passive components. A multi cell hybrid 21-level multilevel inverter is given in [26], [27] with a two-unit topology. The topology generates high output efficiency, low distortion, and reduced electromagnetic interference (EMI) levels. The topology also offers an online method for charging and balancing capacitors without auxiliary circuits. The pulse-width-modulation signals of the 3-level hybrid boost converter based on a single-phase 3-level T-type inverter in [28], [29] is created by comparing two duty cycles and two triangular carrier signals. The converter contains four power switches, four diodes, an inductor, and two capacitors [30]–[32]. Discusses a novel configuration for high gain, high efficiency DC-DC converters that include a single switch, two intermediate capacitors, and a linked inductor for low voltage solar PV module supplied applications. The circuit's structure is designed to lessen the voltage stress on the power device, enhancing efficiency. The proposed work contributes to the field of hybrid converters by incorporating renewable energy sources. Moreover, the efficacy of the proposed system is rigorously validated through simulations conducted in the MATLAB environment.

2. MICROGRID

A micro grid is an amalgamation of at least two environmentally friendly power sources (*i.e.*, solar, wind or fuel cell) which is used to supply the power demand of the consumer. It can be directly used to supply the power to the consumer or it can be used as the secondary power source for the main grid. A micro grid can control itself by using some control strategies such as PQ control, droop control, peer control and decentralized control. Micro grid collects energy from various DG's and supplies that energy to the consumer according to the demand. A DG generates electrical energy, and the generated electrical energy is not transmitted for the longer distances, like solar, wind and small generator that runs on diesel or petrol is used as a distributed generator. There are various challenges associated with integrating distributed energy sources and improving grid stability. Applying multilevel inverters in grid-connected systems overcomes above challenges. Multilevel inverters reduce THD and enhance grid support by generating voltages in multiple levels, reduce filtering requirements, and provide flexibility and scalability.

2.1. Classification of microgrid

Micro grids are grouped into four types in particular. The four types are institutional micro grid, community microgrid, military grade micro grid, and remote off-grid network. Which are described as follows:

- a. Institutional micro grid: the onsite distributive generators are integrated and are controlled by the owner easily in a small area.
- b. Community micro grid: there are 1000s of consumers in this type of micro grid, some of the consumers may have renewable energy sources that are used by them and they generate some excessive amount and that generated excessive amount is being given to the other users who are in need.
- c. Military grade micro grid: used for military activities and these does not depend on the normal grid, this work independently all the time.

- d. Remote off-grid micro grid: this is islanded mode of operation. These types of micro grids are employed where transmission of power from a longer distance is not possible. These work individually from macro grid.

2.2. Induction motor

The induction drive is very comfortable for agricultural modeling in micro grid application because of its high discharge. A DC motor circuit consists of commutator and brushes so that there is a scope of getting frequent sparks, with this reason, the DC motors are normally not preferred in agricultural applications. Because of these reasons generally induction motors are preferred for speed regulated industrial drive applications. Utilizing an induction drive has a few specialized troubles too on the grounds that it requires two supply transformation steps, AC-DC and DC-AC conversions play a critical role in variable-frequency (V/F) control setups. They entail converting AC to DC and vice versa, frequently utilized for motor speed regulation and maintaining specific voltage-to-frequency ratios. Because of its superior electrical properties over different arrangements, turning around voltage topologies with 13 and 21 level converters are regularly utilized in induction drive.

2.3. Induction motor dynamic modeling

For a four-pole machine, the induction drive dynamic modeling comprises of two similar voltage windings. The connections between these windings are antiparallel. These two windings are cut off for the proposed hybrid converter, leaving only the four available terminals. Because of the equivalent dividing between these two windings, the stator resistance, inductance and magnetizing inductance of each similar voltage winding are each equipped for 1/2 the typical voltage value displayed in Figure 1 the accompanying conditions simplify it to analyze the dynamic modeling of a drive.

$$V_{a1} - V_{a2} = \left(\frac{r_s}{2}\right) * i_{as} + \left(\frac{L_{ss}}{2}\right) * i_{as} - \left(\frac{1}{2}\right) * \left(\frac{L_m}{2}\right) * i_{bs} - \left(\frac{1}{2}\right) * \left(\frac{L_m}{2}\right) * i_{cs} \quad (1)$$

$$V_{a3} - V_{a4} = \left(\frac{r_s}{2}\right) * i_{as} + \left(\frac{L_{ss}}{2}\right) * i_{as} - \left(\frac{1}{2}\right) * \left(\frac{L_m}{2}\right) * i_{bs} - \left(\frac{1}{2}\right) * \left(\frac{L_m}{2}\right) * i_{cs} \quad (2)$$

The resultant equivalent voltage is algebraic summation of voltages of (1) and (2).

$$V_{as} = (V_{a1} - V_{a2}) + (V_{a3} - V_{a4}) \quad (3)$$

The per phase voltage of drive can be calculated as (4).

$$V_{as} = r_s * L_{ss} + i_{as} * -\left(\frac{1}{2}\right) * L_m * i_{bs} - \left(\frac{1}{2}\right) * L_m * i_{cs} \quad (4)$$

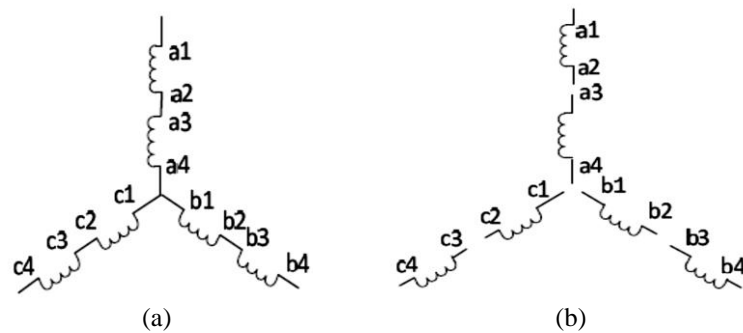


Figure 1. Equivalent (a) stator winding and (b) antiparallel stator winding

In the above method, voltages for other phases can be calculated as (5), (6).

$$V_{bs} = r_s * i_{bs} + L_{ss} * i_{bs} - \left(\frac{1}{2}\right) * L_m * i_{as} - \left(\frac{1}{2}\right) * L_m * i_{cs} \quad (5)$$

$$V_{cs} = r_s * i_{cs} + L_{ss} * i_{cs} - \left(\frac{1}{2}\right) * L_m * i_{as} - \left(\frac{1}{2}\right) * L_m * i_{bs} \quad (6)$$

Voltage conditions in $dq0$ outline is acquired from the overall conditions of induction drive.

$$V_{qs} = r_s * i_{qs} + \omega * \lambda_{ds} + \rho * \lambda_{qs} \quad (7)$$

$$V_{ds} = r_s * i_{ds} - \omega * \lambda_{qs} + \rho * \lambda_{ds} \quad (8)$$

$$V_{0s} = r_s * i_{0s} + \rho * \lambda_{0s} \quad (9)$$

$$V_{qr} = r_r * i_{qr} + (\omega - \omega_r) * \lambda_{dr} + \rho * \lambda_{qr} \quad (10)$$

$$V_{dr} = r_r * i_{dr} - (\omega - \omega_r) * \lambda_{qr} + \rho * \lambda_{dr} \quad (11)$$

$$V_{0r} = r_r * i_{0r} + \rho * \lambda_{0r} \quad (12)$$

Flux linkages are

$$\lambda_{qs} = L_{ss} * i_{qs} + L_m * i_{qr} \quad (13)$$

$$\lambda_{ds} = L_{ss} * i_{ds} + L_m * i_{dr} \quad (14)$$

$$\lambda_{0s} = L_{1s} * i_{0s} \quad (15)$$

$$\lambda_{qr} = L_{rr} * i_{qr} + L_m * i_{qs} \quad (16)$$

$$\lambda_{dr} = L_{rr} * i_{dr} + L_m * i_{ds} \quad (17)$$

$$\lambda_{0r} = L_{1r} * i_{0r} \quad (18)$$

Torque (T_e) as far as $dq0$ current flows is

$$T_e = \left(\frac{3}{2}\right) * \left(\frac{P}{2}\right) * L_m * (i_{qs} * i_{dr} + i_{ds} * i_{qr}) \quad (19)$$

Speed of rotor is

$$\frac{d}{dt} \omega_e = \left(\frac{P}{2*J}\right) * (T_e - T_L) \quad (20)$$

Wherever, d : direct-axis, q : quadrature-axis, s : stator indices, r : rotor indices, P : number of poles, J : moment based on inertia, T_e : electrical torque, T_L : torque. V_{qs}, V_{ds} : stator voltages along the q and d -axes, V_{qr}, V_{dr} : rotor voltages along the q and d -axes, r_r, L_{1r} : rotor resistance, leakage inductance, r_s, L_{1s} : stator resistance, leakage inductance, i_{qs}, i_{ds} : stator currents along the q and d -axes, and i_{qr}, i_{dr} : Rotor currents along the q and d -axes.

The block executes conditions based on a fixed rotor reference (dq) frame. The d -axis coincides with the a -axis. All quantities in the rotor reference frame refer to the stator as represented in Figure 2. These employs the conditions to calculate the electrical speed (ω_{em}) and slip speed (ω_{slip}).

$$\omega_{em} = P\omega_m \quad \omega_{slip} = \omega_{syn} - \omega_{em}$$

Directed toward compute the dq rotor speed regarding the rotor A-hub (dA), the block utilizes the distinction among the stator a -axis (da) speed and slip speed:

$$\omega_{dA} = \omega_{da} - \omega_{em} \quad (21)$$

To improve on the situations for the flux, voltage, and current changes, the block utilizes a fixed note outline:

$$\omega_{da} = 0 \quad \omega_{dA} = -\omega_{em} \quad (22)$$

To improve on the situations for flux, v and I outline:

$$\omega da = 0\omega dA = -\omega em \tag{23}$$

The flux equations can be describing as,

$$\frac{d}{dt} \begin{bmatrix} \lambda_{sd} \\ \lambda_{sq} \end{bmatrix} = \begin{bmatrix} V_{sd} \\ V_{sq} \end{bmatrix} - R_s \begin{bmatrix} i_{sd} \\ i_{sq} \end{bmatrix} - W_{da} \begin{bmatrix} 0 & -1 \\ 1 & 0 \end{bmatrix} \begin{bmatrix} \lambda_{sd} \\ \lambda_{sq} \end{bmatrix}$$

$$\frac{d}{dt} \begin{bmatrix} \lambda_{rd} \\ \lambda_{rq} \end{bmatrix} = \begin{bmatrix} V_{rd} \\ V_{rq} \end{bmatrix} - R_r \begin{bmatrix} i_{rd} \\ i_{rq} \end{bmatrix} - W_{dA} \begin{bmatrix} 0 & -1 \\ 1 & 0 \end{bmatrix} \begin{bmatrix} \lambda_{rd} \\ \lambda_{rq} \end{bmatrix}$$

$$\begin{bmatrix} \lambda_{sd} \\ \lambda_{sq} \\ \lambda_{rd} \\ \lambda_{rq} \end{bmatrix} = \begin{bmatrix} L_s & 0 & L_m & 0 \\ 0 & L_s & 0 & L_m \\ L_m & 0 & L_r & 0 \\ 0 & L_m & 0 & L_r \end{bmatrix} \begin{bmatrix} i_{sd} \\ i_{sq} \\ i_{rd} \\ i_{rq} \end{bmatrix}$$

Current is given by:

$$\begin{bmatrix} i_{sd} \\ i_{sq} \\ i_{rd} \\ i_{rq} \end{bmatrix} = \left(\frac{1}{L_m^2 - L_r L_s} \right) \begin{bmatrix} -L_s & 0 & L_m & 0 \\ 0 & -L_s & 0 & L_m \\ L_m & 0 & -L_r & 0 \\ 0 & L_m & 0 & -L_r \end{bmatrix} \begin{bmatrix} \lambda_{sd} \\ \lambda_{sq} \\ \lambda_{rd} \\ \lambda_{rq} \end{bmatrix}$$

Inductance is given by

$$L_s = L_{ls} + L_m; L_r = L_{lr} + L_m$$

Power constant dq change to guarantee that the dq and 3-stage powers are equivalent and the corresponding voltage equations are given by

$$\begin{bmatrix} V_{sd} \\ V_{sq} \end{bmatrix} = \sqrt{\frac{2}{3}} \begin{bmatrix} \cos(\theta_{da}) & \cos(\theta_{da} - \frac{2\pi}{3}) & \cos(\theta_{da} + \frac{2\pi}{3}) \\ -\sin(\theta_{da}) & -\sin(\theta_{da} - \frac{2\pi}{3}) & -\sin(\theta_{da} + \frac{2\pi}{3}) \end{bmatrix} \begin{bmatrix} V_a \\ V_b \\ V_c \end{bmatrix}$$

$$\begin{bmatrix} i_a \\ i_b \\ i_c \end{bmatrix} = \sqrt{\frac{2}{3}} \begin{bmatrix} \cos(\theta_{da}) & -\sin(\theta_{da}) \\ \cos(\theta_{da} - \frac{2\pi}{3}) & -\sin(\theta_{da} - \frac{2\pi}{3}) \\ \cos(\theta_{da} + \frac{2\pi}{3}) & -\sin(\theta_{da} + \frac{2\pi}{3}) \end{bmatrix} \begin{bmatrix} i_{sd} \\ i_{sq} \end{bmatrix}$$

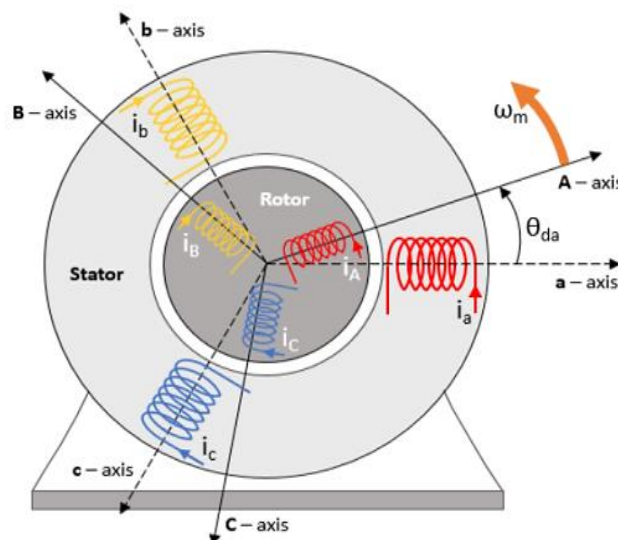


Figure 2. Stator and rotor circuit of induction drive

3. SYSTEM BLOCK DIAGRAM OF A HYBRID INVERTER CONNECTED TO INDUCTION DRIVE

The block diagram shown in Figure 3 illustrates the system representation for a novel photovoltaic (PV) based single-stage 13-level and 21-level hybrid H-bridge inverter (HHBI). It is connected to an induction motor. Here, the input of the induction motor is linked to the output of an inverter by using smoothing reactors.

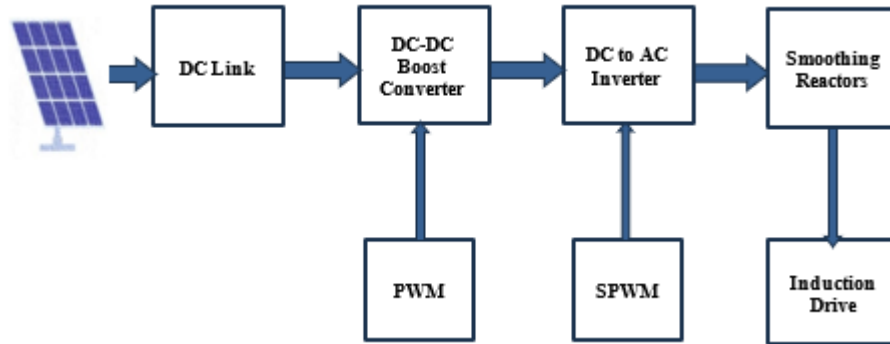


Figure 3. System block diagram for a novel PV hybrid inverter fed to motor drive

3.1. 13-level novel hybrid inverter topology

Figure 4 illustrates the circuit topology of a novel PV-based 13-level hybrid inverter. The corresponding rearrangement sequence is detailed in Table 1 and modes of exchanging voltage from 0 to V_{dc} in Table 2. The switching operations of 13-level hybrid inverter are given in Figure 5, with voltage level '0' in Figure 5(a) and voltage level $V_{dc}/6$ in Figure 5(b) for implementation of topology.

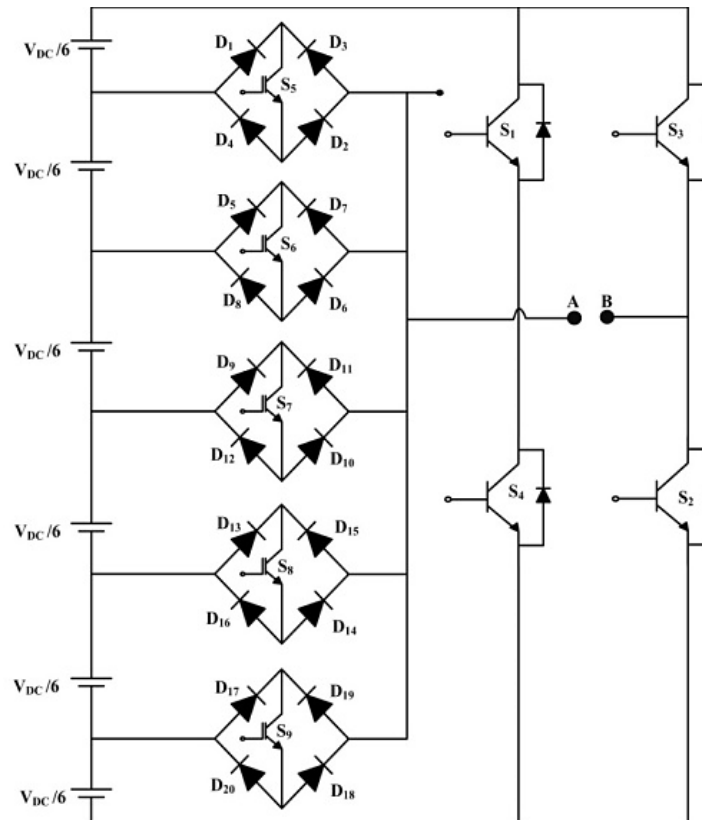


Figure 4. Novel PV based hybrid inverter topology

Table 1. Working sequence of an inverter

Voltage level	S1	S2	S3	S4	S5	S6	S7	S8	S9
0	0	1	0	1	0	0	0	0	0
$V_{DC}/6$	0	1	0	0	0	0	0	0	1
$V_{DC}/3$	0	1	0	0	0	0	0	1	0
$V_{DC}/2$	0	1	0	0	0	0	1	0	0
$2V_{DC}/3$	0	1	0	0	0	0	1	0	0
$5V_{DC}/6$	0	1	0	0	1	0	0	0	0
V_{DC}	1	1	0	0	0	0	0	0	0
$-V_{DC}/6$	0	0	1	0	1	0	0	0	0
$-V_{DC}/3$	0	0	1	0	0	1	0	0	0
$-V_{DC}/2$	0	0	1	0	0	0	1	0	0
$-2V_{DC}/3$	0	0	1	0	0	0	0	1	0
$-5V_{DC}/6$	0	0	1	0	0	0	0	0	1
$-V_{DC}$	1	0	1	0	0	0	0	0	0

Table 2. Gives the modes of exchanging voltage from 0 to V_{dc}

S. No	Voltage level	Current direction
1	0	S4-A-B-S2
2	$V_{DC}/6$	$V_{DC}/6^+-D_{17}-S_{09}-D_{18}-A-B-S_2-V_{DC}/6^-$
3	$V_{DC}/3$	$V_{DC}/6^+-D_{13}-S_{08}-D_{14}-A-B-S_2-V_{DC}/6^-$
4	$V_{DC}/2$	$V_{DC}/6^+-D_{09}-S_{07}-D_{10}-A-B-S_2-V_{DC}/6^-$
5	$2V_{DC}/3$	$V_{DC}/6^+-D_{05}-S_{06}-D_{06}-A-B-S_2-V_{DC}/6^-$
6	$5V_{DC}/6$	$V_{DC}/6^+-D_{01}-S_{05}-D_{02}-A-B-S_2-V_{DC}/6^-$
7	V_{DC}	A-S1-B-S2

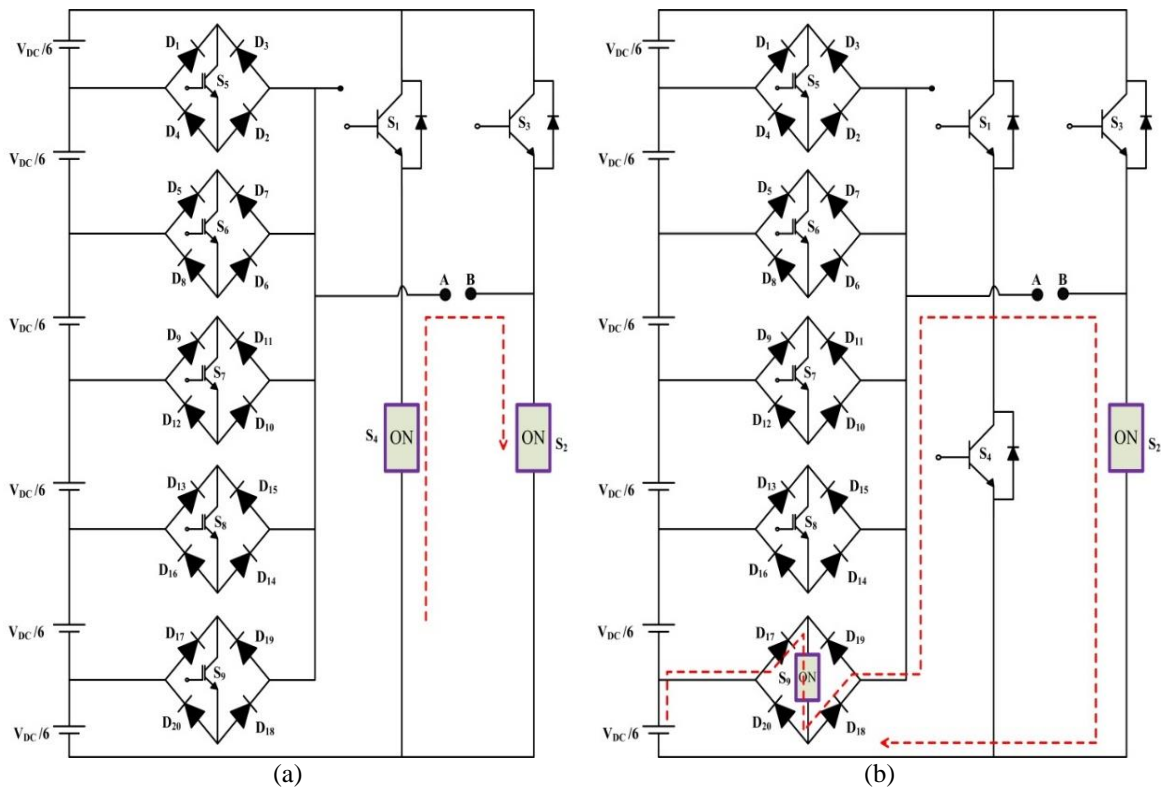


Figure 5. Switching operations of 13 level hybrid inverter with (a) '0' voltage level and (b) $V_{DC}/6$ voltage level

3.2. Simulink wave forms of a novel PV based 3-phase 13-level HHBI fed to induction drive

Figures 6 to 10 represent Simulink wave forms of a novel PV based 3-phase 13-level HHBI fed to induction drive. It can be observed from above wave forms that with 13-level HHBI the THD has been reduced to 7.41% and the voltage, current and speed wave forms reach steady state at 0.3 sec after the transients.

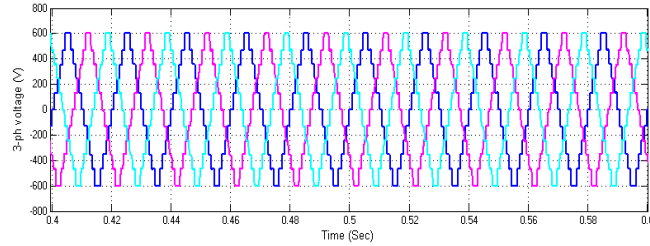


Figure 6. Voltage wave form of an induction drive

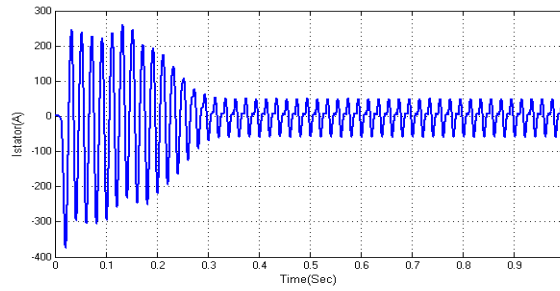


Figure 7. Stator current of an induction drive

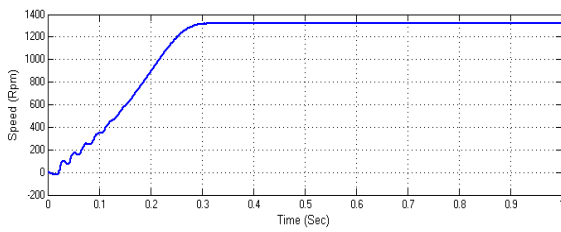


Figure 8. Speed wave form

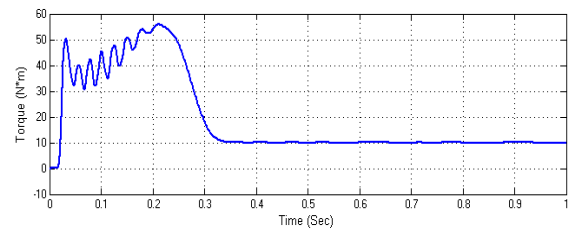


Figure 9. T-Characteristics of induction drive

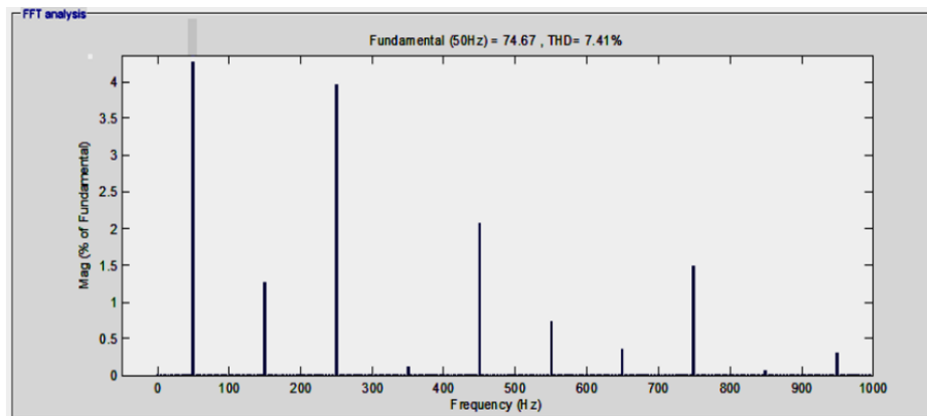


Figure 10. THD of induction drive

4. PROPOSED 21-LEVEL HYBRID H-BRIDGE INVERTER

In this configuration 10 DC voltage supplies are utilized with $V_{DC}/10$. Figure 11 addresses circuit topology for 21-level HHBI and the switching activity is given in Table 3. Table 4 gives the various current paths for voltage levels 0 to V_{DC} HHBI based on the states of the converter elements. The elements which are conducted at different time intervals are presented in Table 4.

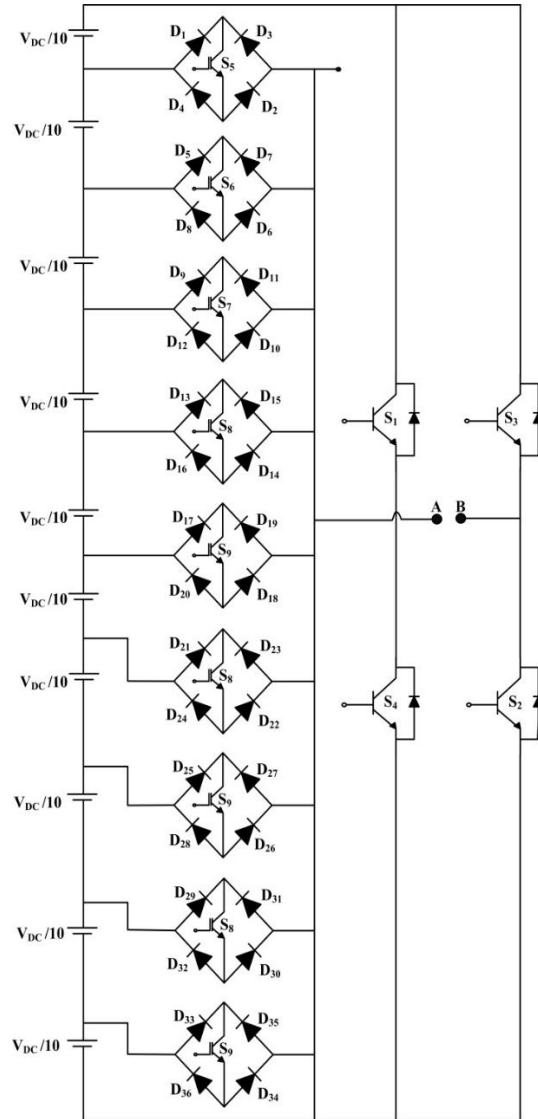


Figure 11. 21-level hybrid inverter topology's

Table 3. Switching order of a 21-level HHBI

Voltage level	S1	S2	S3	S4	S5	S6	S7	S8	S9	S10	S11	S12	S13
0	0	1	0	1	0	0	0	0	0	0	0	0	0
$V_{DC}/10$	0	1	0	0	0	0	0	0	0	0	0	0	1
$2V_{DC}/10$	0	1	0	0	0	0	0	0	0	0	0	1	0
$3V_{DC}/10$	0	1	0	0	0	0	0	0	0	0	1	0	0
$4V_{DC}/10$	0	1	0	0	0	0	0	0	0	1	0	0	0
$5V_{DC}/10$	0	1	0	0	0	0	0	0	1	0	0	0	0
$6V_{DC}/10$	0	1	0	0	0	0	0	1	0	0	0	0	0
$7V_{DC}/10$	0	1	0	0	0	0	1	0	0	0	0	0	0
$8V_{DC}/10$	0	1	0	0	0	1	0	0	0	0	0	0	0
$9V_{DC}/10$	0	1	0	0	1	0	0	0	0	0	0	0	0
V_{DC}	1	1	0	0	0	0	0	0	0	0	0	0	0
$-V_{DC}/10$	0	0	1	0	1	0	0	0	0	0	0	0	0
$-2V_{DC}/10$	0	0	1	0	0	1	0	0	0	0	0	0	0
$-3V_{DC}/10$	0	0	1	0	0	0	1	0	0	0	0	0	0
$-4V_{DC}/10$	0	0	1	0	0	0	0	1	0	0	0	0	0
$-5V_{DC}/10$	0	0	1	0	0	0	0	0	1	0	0	0	0
$-6V_{DC}/10$	0	0	1	0	0	0	0	0	0	1	0	0	0
$-7V_{DC}/10$	0	0	1	0	0	0	0	0	0	0	1	0	0
$-8V_{DC}/10$	0	0	1	0	0	0	0	0	0	0	0	1	0
$-9V_{DC}/10$	0	0	1	0	0	0	0	0	0	0	0	0	1
$-V_{DC}$	0	0	1	1	0	0	0	0	0	0	0	0	0

Table 4. Voltages and current paths for different time intervals

S. No.	Voltage level	Current direction
1	0	S4-A-B-S2
2	$V_{DC}/10$	$V_{DC}/10^+$ -D ₃₃ -S13-D ₃₄ -A-B-S2- $V_{DC}/10^-$
3	$2V_{DC}/10$	$V_{DC}/10^+$ -D ₂₉ -S12-D ₃₀ -A-B-S2- $V_{DC}/10^-$
4	$3V_{DC}/10$	$V_{DC}/10^+$ -D ₂₅ -S11-D ₂₆ -A-B-S2- $V_{DC}/10^-$
5	$4V_{DC}/10$	$V_{DC}/10^+$ -D ₂₁ -S10-D ₂₂ -A-B-S2- $V_{DC}/10^-$
6	$5V_{DC}/10$	$V_{DC}/10^+$ -D ₁₇ -S09-D ₁₈ -A-B-S2- $V_{DC}/10^-$
7	$6V_{DC}/10$	$V_{DC}/10^+$ -D ₁₃ -S08-D ₁₄ -A-B-S2- $V_{DC}/10^-$
8	$7V_{DC}/10$	$V_{DC}/10^+$ -D ₀₉ -S07-D ₁₀ -A-B-S2- $V_{DC}/10^-$
9	$8V_{DC}/10$	$V_{DC}/10^+$ -D ₀₅ -S06-D ₀₆ -A-B-S2- $V_{DC}/10^-$
10	$9V_{DC}/10$	$V_{DC}/10^+$ -D ₀₁ -S05-D ₀₂ -A-B-S2- $V_{DC}/10^-$
11	V_{DC}	A-S1-B-S2

In this 10 DC voltage source, entire $V_{DC}/10$ is used. There are 13 switches in all, with just two switches in the ON position for each voltage level. The voltage levels for positive orientation are 0, $V_{DC}/10$, $2 V_{DC}/10$, $3 V_{DC}/10$, $4 V_{DC}/10$, $5 V_{DC}/10$, $6 V_{DC}/10$, $7 V_{DC}/10$, $8 V_{DC}/10$, $9 V_{DC}/10$, and V_{DC} , while corresponding voltages for negative orientations are denoted by a negative sign. The voltage change rate (dV/dt) at each level is $V_{DC}/10$. As a result, pressure on switches is reduced significantly. Figures 12 (a) and 12(b) shows the actual path for positive voltage levels of the 21-level HHBI.

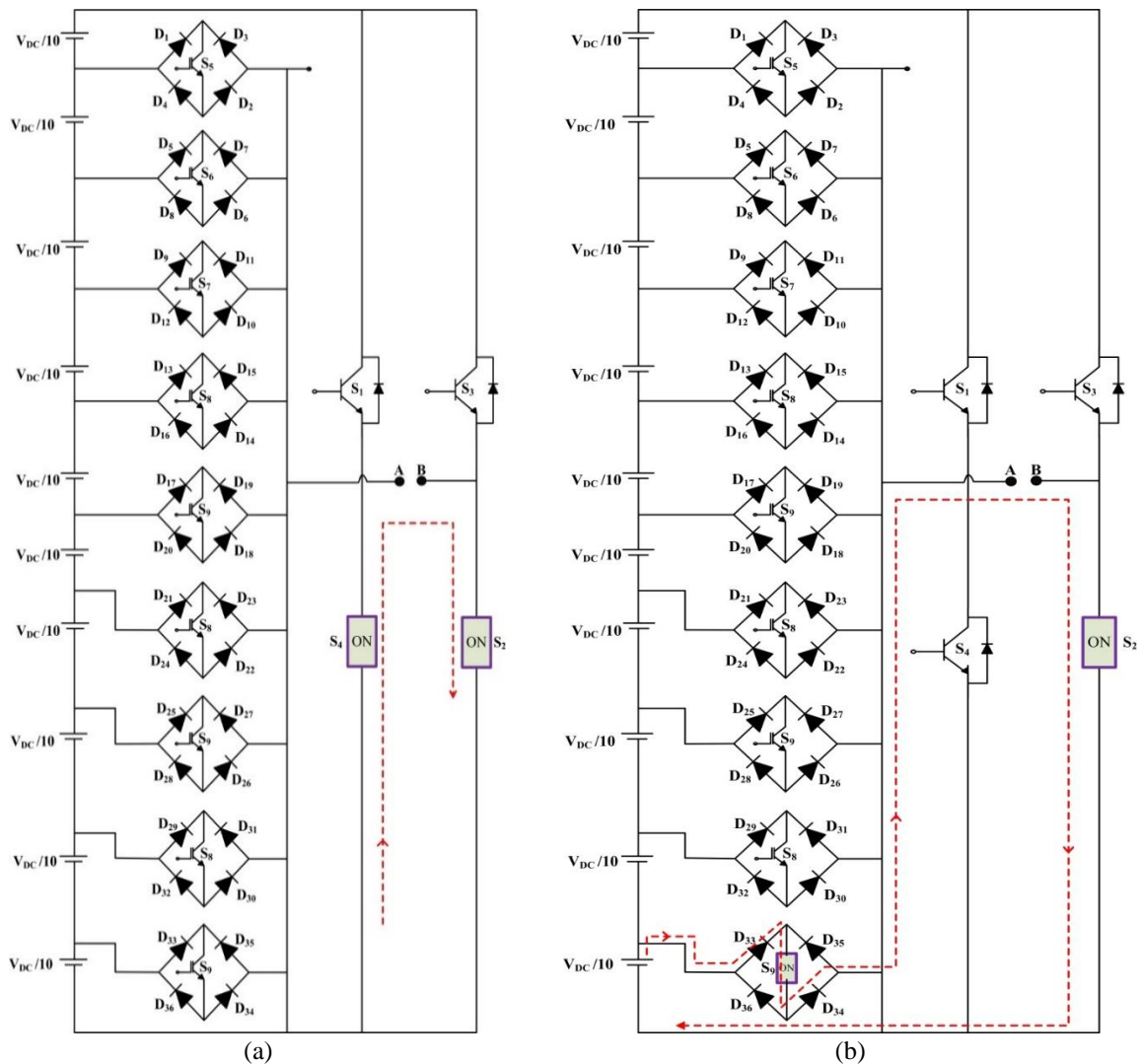


Figure 12. 3-phase 21-level HHBI fed to induction drive, conduction of devices for (a) ‘0’ voltage level and (b) $V_{DC}/10$ voltage level

4.1. Simulink wave forms of a novel PV based 3-phase 21-level HHBI fed to induction drive

The implemented novel PV based 3-phase 21-level HHBI fed to induction drive output waveforms are shown in Figures 13 to 17. From the outputs wave forms of 21-level HHBI, THD has been reduced to 4.66% and the resulted voltage, current and speed of the drive system are within the prescribed limits. The implemented 13 and 21-level HHDI topologies are compared on the basic of switches and THD as given in Table 5.

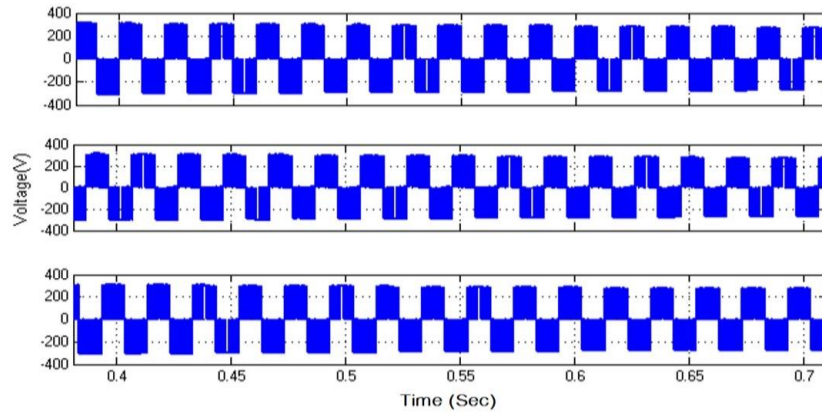


Figure 13. Voltage waveforms of inverter phase leg

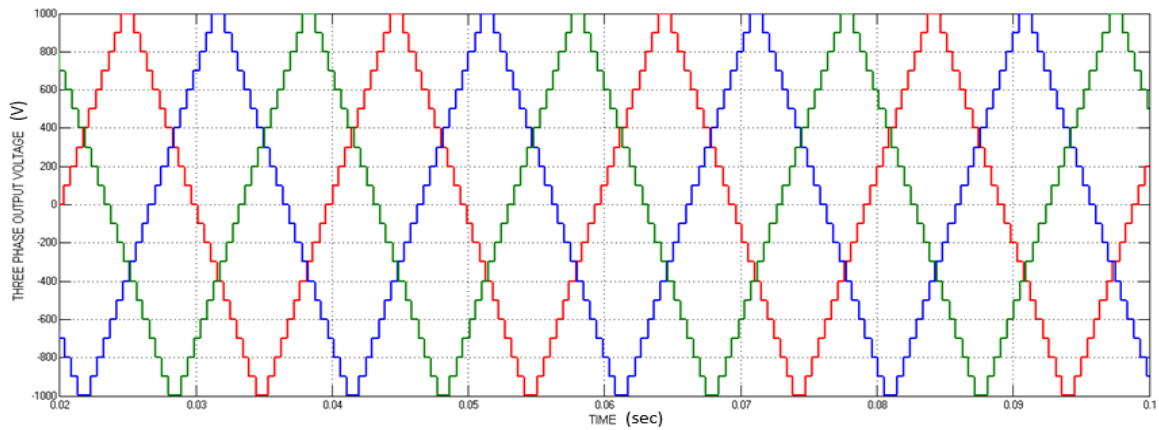


Figure 14. 21-level o/p voltage of proposed three-stage HHBI

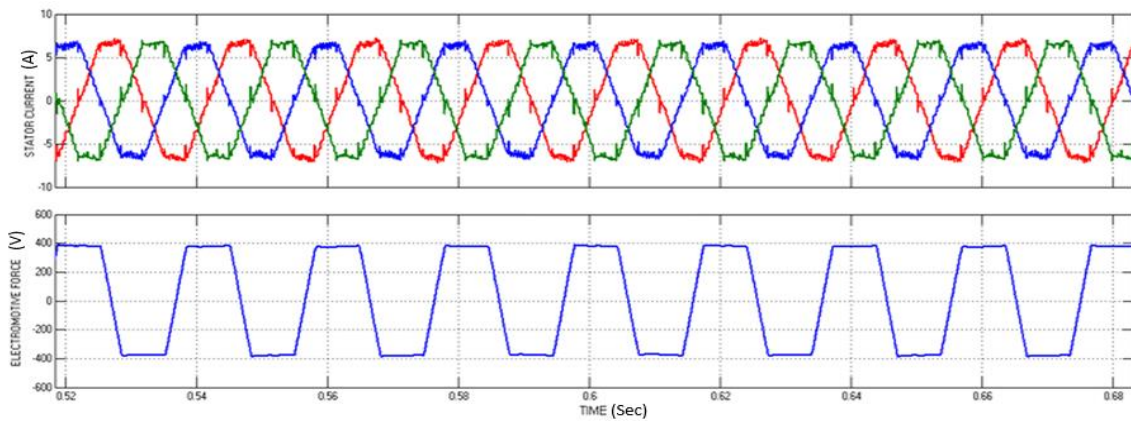


Figure 15. Stator current, electromotive force

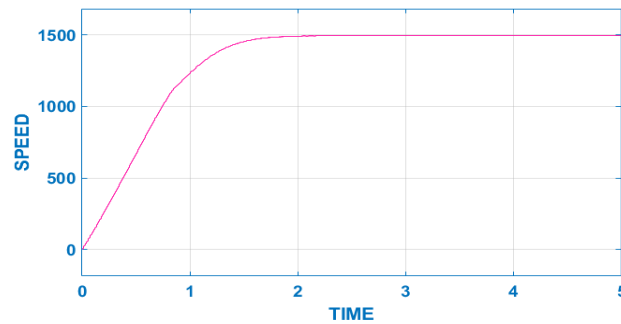


Figure 16. Speed (N) of induction drive

Table 5. Comparison of results

S. No.	Parameter	3-phase hybrid H-bridge inverter -13 level [29]	3-phase recommend hybrid H-bridge inverter -21 level [26]–[28]
1	No. of switches	27	39
2	No. of DC supply voltages	18	27
3	Total THD%	7.41	4.66

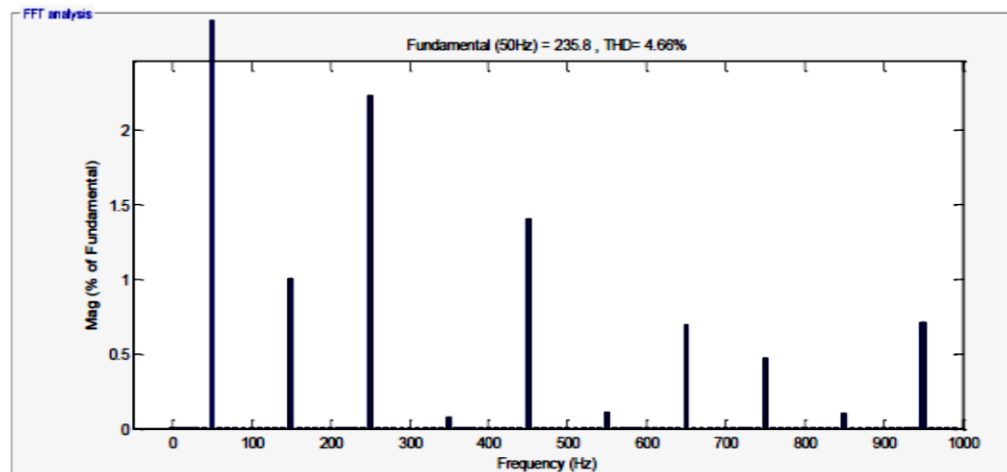


Figure 17. THD for 21-level inverter

5. CONCLUSION

This paper presents a novel 3-phase 13 and 21-level Hybrid H-Bridge Inverter related with induction drive by including X/R ratio for loading condition. From the modelling equations, Simulink implementation and its results, it is evident that as the level of output voltage increases, the total THD value decreases. Simultaneously the utilization of the prerequisite of the number switches and their particular driver circuits for planning the topology is additionally increments. The novel topology of HHBI reduced the number of switches when compared with all the conventional topologies in the literature. Subsequently, H-Bridge inverter fed induction machine adds more benefits in real time applications. The number of switches are minimized to 39 and the voltage THD value is reduced to 4.66%, and the initial transients are vanished within the limits.




REFERENCES

- [1] N. Sandeep and U. R. Yaragatti, "Design and implementation of active neutral point-clamped nine-level reduced device count inverter: an application to grid integrated renewable energy sources," *IET Power Electronics*, vol. 11, no. 1, pp. 82–91, 2018, doi: 10.1049/iet-pel.2016.0951.
- [2] N. K. Reddi, M. R. Ramteke, H. M. Suryawanshi, K. Kothapalli, and S. P. Gawande, "An isolated multi-input ZCS DC–DC front-end-converter based multilevel inverter for the integration of renewable energy sources," *IEEE Transactions on Industry Applications*, vol. 54, no. 1, pp. 494–504, 2018, doi: 10.1109/TIA.2017.2753160.




- [3] R. Agrawal and S. Jain, "Multilevel inverter for interfacing renewable energy sources with low/medium-and high voltage grids," *IET Renewable Power Generation*, vol. 11, no. 14, pp. 1822–1831, 2017, doi: 10.1049/iet-rpg.2016.1034.
- [4] A. M. Noman, K. E. Addoweesh, A. A. Alabduljabbar, and A. I. Alolah, "Cascaded H-bridge MLI and three-phase cascaded VSI topologies for grid-connected PV systems with distributed MPPT," *International Journal of Photoenergy*, vol. 2019, 2019, doi: 10.1155/2019/7642919.
- [5] S. Shuvo, E. Hossain, T. Islam, A. Akib, S. Padmanaban, and M. Z. R. Khan, "Design and hardware implementation considerations of modified multilevel cascaded H-bridge inverter for photovoltaic system," *IEEE Access*, vol. 7, pp. 16504–16524, 2019, doi: 10.1109/ACCESS.2019.2894757.
- [6] S. Jain and V. Sonti, "A highly efficient and reliable inverter configuration based cascaded multilevel inverter for PV systems," *IEEE Transactions on Industrial Electronics*, vol. 64, no. 4, pp. 2865–2875, 2017, doi: 10.1109/TIE.2016.2633537.
- [7] M. R. Nayaka, M. Sarithab, S. A. Mujeerc, B. Devulal, and T. S. Kumar, "A photovoltaic based multilevel inverter fed induction motor drive," *Turkish Journal of Computer and Mathematics Education (TURCOMAT)*, vol. 12, no. 10, pp. 6196–6212, Apr. 2021, doi: 10.17762/turcomat.v12i10.5459.
- [8] J. Sastry, P. Bakas, H. Kim, L. Wang, and A. Marinopoulos, "Evaluation of cascaded H-bridge inverter for utility-scale photovoltaic systems," *Renewable Energy*, vol. 69, pp. 208–218, 2014, doi: 10.1016/j.renene.2014.03.049.
- [9] X. Guo, R. He, and M. Narimani, "Modeling and analysis of new multilevel inverter for solar photovoltaic power plant," *International Journal of Photoenergy*, vol. 2016, 2016, doi: 10.1155/2016/4063167.
- [10] C. Dhanamjayulu and T. Girijaprasanna, "Experimental implementation of cascaded H-bridge multilevel inverter with an improved reliability for solar PV applications," *International Transactions on Electrical Energy Systems*, vol. 2023, 2023, doi: 10.1155/2023/8794874.
- [11] C. Kannan, N. K. Mohanty, and R. Selvarasu, "A new topology for cascaded H-bridge multilevel inverter with PI and fuzzy control," *Energy Procedia*, vol. 117, pp. 917–926, 2017, doi: 10.1016/j.egypro.2017.05.211.
- [12] C. P. Sekhar, P. V. R. Rao, and M. U. Vani, "Novel multilevel inverter with minimum number of switches," in *Proceedings - 2017 International Conference on Recent Trends in Electrical, Electronics and Computing Technologies, ICRTEECT 2017*, 2017, vol. 2017-Decem, pp. 106–112, doi: 10.1109/ICRTEECT.2017.44.
- [13] B. Devulal, M. Siva, D. R. Kumar, and V. Rajashekar, "Design and analysis of micro-grid stability with various DGs," *Lecture Notes in Electrical Engineering*, vol. 893 LNEE, pp. 406–414, 2022, doi: 10.1007/978-981-19-1742-4_34.
- [14] B. Devulal, M. Siva, and D. Ravi Kumar, "Design of a novel converter topology for micro grid applications," *Journal of Electrical Systems*, vol. 20, no. 2, pp. 2428–2449, 2024, doi: 10.52783/jes.2017.
- [15] J. H. Latha and B. R. Banakara, "Modeling and analysis of 21 level cascade model multilevel inverter," in *2018 2nd International Conference on Inventive Systems and Control (ICISC)*, Jan. 2018, pp. 586–591, doi: 10.1109/ICISC.2018.8398867.
- [16] B. Sahan, S. V. Araújo, C. Nöding, and P. Zacharias, "Comparative evaluation of three-phase current source inverters for grid interfacing of distributed and renewable energy systems," *IEEE Transactions on Power Electronics*, vol. 26, no. 8, pp. 2304–2318, Aug. 2011, doi: 10.1109/TPEL.2010.2096827.
- [17] A. Agarwal and N. Kumar, "Reduced stage three phase multisource hybrid converter for integration of PV and grid power," *Sustainable Energy Technologies and Assessments*, vol. 62, 2024, doi: 10.1016/j.seta.2024.103608.
- [18] S. Saponara, R. Saletti, and L. Mihet-Popa, "Hybrid micro-grids exploiting renewables sources, battery energy storages, and bi-directional converters," *Applied Sciences (Switzerland)*, vol. 9, no. 22, 2019, doi: 10.3390/APP9224973.
- [19] S. M. Sharkh, M. A. Abusara, G. I. Orfanoudakis, and B. Hussain, *Power electronic converters for microgrids*. Wiley, 2014, doi: 10.1002/9780470824054.
- [20] M. di Benedetto, A. Lidozzi, L. Solero, F. Crescimbin, and P. J. Grbović, "High-Performance 3-Phase 5-Level E-Type Multilevel-Multicell Converters for Microgrids," *Energies*, vol. 14, no. 4, pp. 1–21, Feb. 2021, doi: 10.3390/en14040843.
- [21] S. Dasgupta, S. N. Mohan, S. K. Sahoo, and S. K. Panda, "Application of four-switch-based three-phase grid-connected inverter to connect renewable energy source to a generalized unbalanced microgrid system," *IEEE Transactions on Industrial Electronics*, vol. 60, no. 3, pp. 1204–1215, Mar. 2013, doi: 10.1109/TIE.2012.2202350.
- [22] X. Shen, D. Tan, Z. Shuai, and A. Luo, "Control techniques for bidirectional interlinking converters in hybrid microgrids: leveraging the advantages of both AC and DC," *IEEE Power Electronics Magazine*, vol. 6, no. 3, pp. 39–47, 2019, doi: 10.1109/mpel.2019.2925298.
- [23] S. U. Ali *et al.*, "Model predictive control—based distributed control algorithm for bidirectional interlinking converter in hybrid microgrids," *International Transactions on Electrical Energy Systems*, vol. 31, no. 10, 2021, doi: 10.1002/2050-7038.12817.
- [24] Q. Qi, D. Ghaderi, and J. M. Guerrero, "Sliding mode controller-based switched-capacitor-based high DC gain and low voltage stress DC-DC boost converter for photovoltaic applications," *International Journal of Electrical Power and Energy Systems*, vol. 125, 2021, doi: 10.1016/j.ijepes.2020.106496.
- [25] D. Ertekin, "ARVIN converter: a bidirectional DC/DC converter for grid-connected G2V/V2G energy storage and electrification approaches," *Electrical Engineering*, 2024, doi: 10.1007/s00202-024-02295-x.
- [26] A. Hassan, X. Yang, and W. Chen, "A multi-cell 21-level hybrid multilevel inverter synthesizes a reduced number of components with voltage boosting property," *IEEE Access*, vol. 8, pp. 224439–224451, 2020, doi: 10.1109/ACCESS.2020.3044268.
- [27] J. S. Rao, P. S. Varma, and T. S. Kumar, "Novel switching design structure for three phase 21-level multilevel inverter fed BLDC drive application," *International Journal of Power Electronics and Drive Systems*, vol. 9, no. 3, pp. 1202–1213, 2018, doi: 10.11591/ijpeds.v9.i3.pp1202-1213.
- [28] N. Osman, M. F. Mohamad Elias, and N. A. Rahim, "Design and analysis of three-level hybrid boost converter based on T-type inverter for solar photovoltaic system," *IET Power Electronics*, vol. 13, no. 9, pp. 1848–1857, Jul. 2020, doi: 10.1049/iet-pel.2019.1088.
- [29] S. Sabyasachi, V. B. Borghate, and S. K. Maddugari, "A 13-level hybrid multilevel inverter topology by combining ANPC and improved H-bridge," *IECON Proceedings (Industrial Electronics Conference)*, vol. 2019-Octob, pp. 4947–4952, 2019, doi: 10.1109/IECON.2019.8926810.
- [30] M. Das, M. Pal, and V. Agarwal, "Novel high gain, high efficiency DC-DC converter suitable for solar PV module integration with three phase grid tied inverters," *IEEE Journal of Photovoltaics*, vol. 9, no. 2, pp. 528–537, 2019, doi: 10.1109/JPHOTOV.2018.2877006.
- [31] C.-H. Hsieh, T.-J. Liang, S.-M. Chen, and S.-W. Tsai, "Design and Implementation of a novel multilevel DC-AC inverter," *IEEE Transactions on Industry Applications*, vol. 52, no. 3, pp. 2436–2443, May 2016, doi: 10.1109/TIA.2016.2527622.
- [32] E. Bushra, K. Zeb, I. Ahmad, and M. Khalid, "A comprehensive review on recent trends and future prospects of PWM techniques for harmonic suppression in renewable energies based power converters," *Results in Engineering*, vol. 22, 2024, doi: 10.1016/j.rineng.2024.102213.

BIOGRAPHIES OF AUTHORS






Bhukya Devulal    completed his B.E in electrical and electronics engineering from Sir CR Reddy College of engineering in Eluru, Andhra University. M.Tech. in high voltage engineering from JNTU Kakinada. Pursuing Ph.D. from Annamalai University. Completed “Graduate engineer course in operation and maintenance of electrical power transmission and distribution system” conducted by National Power Training Institute (NPTI), Nagpur. Worked as Site Engineer for one year in “Rural Electrification Corporation Limited” (RECPDCL) under the Ministry of Power Quality Inspection of Village Electrification works through RGGVY scheme. Research interests are power systems, high voltage, renewable energy systems and microgrids. He has 10 Years of teaching experience. He published 11 research papers in International, National Journals and Conferences. He also published two Patents. Department of Science and Technology (DST) Granted Rs. 9 Lakhs for conduction of FDP in AI based power systems. He is currently working as an assistant professor in the Department of Electrical and Electronics Engineering and Dept. Placement Coordinator of VNR Vignana Jyothi Institute of Engineering and Technology, Hyderabad, India. He can be contacted at email: devulal_b@vnrvjiet.in.



Manickam Siva    completed his B.E. in EEE in 1999 from SRM Engineering College (Madras University), M.E. in power systems from Annamalai University, Annamalainagar in 2008 and Ph.D. in electrical and electronics engineering from Annamalai University, Annamalainagar in 2019. He has 22 Years of teaching experience. He has published 7 research papers in International, National Journals and Conferences. Some of his papers are indexed by Scopus and Web of Science. He is currently working as an assistant professor on deputation in the Department of Electrical and Electronics Engineering and Department In Charge of Government Polytechnic College, Cheyyar, Tiruvannamalai, India. He can be contacted at email: vasi.siva@gmail.com.



Dasari Ravi Kumar    completed his B.Tech. in EEE in 2006 and M.Tech. in power systems from JNTU, Hyderabad in 2008 and Ph.D. in electrical engineering from JNTU Anantapur in 2017. He has 16 Years of teaching experience. He has published 47 research papers in International, National Journals and Conferences. He visited Singapore and presented a paper in IEEE International Conference ICBEST-2015 at CREATE, Singapore. Some of his papers are indexed by Scopus and Web of Science. He has Published 4 Patents. He has executed UGC Minor Research Project on "Development of optimization techniques for protective devices and distributed generators allocation to optimize Reliability and to reduce losses in electrical power distribution systems with a sanctioned amount of Rs. 4.95 Lakhs". He has executed a consultancy project with HBL Power Systems Ltd. with an amount of Rs. 7.48 Lakhs. He received Tier-1 Award from IEEE Reliability Society at Eastern Washington University, USA. He is currently working as an associate professor in the Department of Electrical and Electronics Engineering and Incharge-PAAC of VNR Vignana Jyothi Institute of Engineering and Technology, Hyderabad, India. He can be contacted at email: ravikumar_d@vnrvjiet.in.